Journal of Physiology (1993), **460**. *pp.* 91–116
With 14 *figures*
Printed in Great Britain

THE WHOLE-CELL CALCIUM CURRENT IN ACUTELY DISSOCIATED MAGNOCELLULAR CHOLINERGIC BASAL FOREBRAIN NEURONES OF THE RAT

BY T. G. J. ALLEN*, J. A. SIM AND D. A. BROWN

From the Department of Pharmacology, University College London, Gower Street, London WC1E 6BT

(*Received 2 March 1992*)

SUMMARY

1. The electrophysiological and pharmacological characteristics of the calcium current (I_{Ca}) in acutely dissociated magnocellular cholinergic basal forebrain neurones from 11- to 14-day-old post-natal rats were studied using the whole-cell patch-clamp technique.

2. All cells exhibited a small transient low-voltage-activated (LVA) current with half-activation and half-inactivation potentials of −40·2 and −49·3 mV and slope factors for activation and inactivation of 4·82 and 3·85 mV per e-fold change in membrane potential (V_m) respectively. Activation and inactivation rates for the LVA current were highly voltage dependent. For test potential changes from −50 to −20 mV, the time-to-peak of the current decreased from 39·1 to 6·4 ms, and the time constant of current decay decreased from 81·7 to 15·5 ms.

3. A high-voltage-activated (HVA) component of I_{Ca} could be elicited at threshold voltages between −46 and −30 mV from a holding potential (V_H) of −80 mV. The HVA current peaked around 0 mV; a 10-fold increase in $[Ca^{2+}]_o$ produced a 13 mV positive shift in the peak, whilst the amplitude of the current showed an approximately hyperbolic relationship to $[Ca^{2+}]_o$ with half-saturation at 2·5 mM. The transient phase of the HVA current could be described by two exponential functions with time constants τ_{fast} and τ_{slow} of 16·2 and 301 ms. Steady-state inactivation of the transient and extrapolated true sustained (pedestal) components of HVA current were described by Boltzmann equations, with half-inactivation potentials (slope factors) of −47·3 mV, (9·04) and −29·2 mV (11·8) respectively.

4. ω-Conotoxin (ω-CgTX; 100 nM) irreversibly inhibited a kinetically distinct component of HVA current but had no effect upon the transient LVA current. The ω-CgTX-sensitive current could not be distinguished from the control HVA current by the voltage dependence of its activation or inactivation rates.

5. Low concentrations of amiloride ($\leqslant 300\ \mu M$) or Ni^{2+} ($\leqslant 5\ \mu M$) selectively inhibited the transient LVA current, with IC_{50} values of 97 and 5 μM respectively. Cd^{2+} ($\leqslant 1\ \mu M$) selectively blocked a component of HVA current. At higher concentrations, Cd^{2+} and Ni^{2+} were non-selective and totally blocked all components of I_{Ca}.

* To whom correspondence should be addressed.

MS 1164

6. The lanthanide ions Gd^{3+} and La^{3+} produced saturable incomplete block of the HVA current. Maximally effective concentrations of Gd^{3+} (100 μM) or La^{3+} (30 μM) inhibited 76·5 and 41·2% respectively of the sustained component of HVA current with corresponding IC_{50} values of 2·2 and 1·1 μM. Low concentrations of Gd^{3+} ($\leqslant 3$ μM) and La^{3+} ($\leqslant 1$ μM) blocked a substantial component of the HVA current that was pharmacologically distinct from the ω-CgTX-sensitive current.

7. The transient LVA current was inhibited by dihydropyridine (DHP) calcium channel antagonists. The order of potency was nicardipine > nimodipine = nitrendipine > nifedipine. The corresponding apparent IC_{50} values were 0·77, 8·2 and 97 μM. Bay K 8644 (1–3 μM) did not potentiate the LVA current.

8. DHP antagonists produced a dose-dependent block of the sustained component of HVA current. The order of potency was nicardipine > nitrendipine > nimodipine > nifedipine with corresponding IC_{50} values of 7, 14, 61 and 200 μM.

9. Bay K 8644 (1–3 μM) produced a small enhancement (11·3% at 0 mV) of the HVA current at test potentials between -55 and 0 mV (V_H -80 mV). The Bay K enhancement of the current was totally antagonized by concentrations of nifedipine (1–5 μM) that produced little block of the control HVA current.

10. These results show that the calcium current in rat magnocellular cholinergic basal forebrain neurones was composed of LVA and multiple HVA currents which display distinct kinetic and pharmacological characteristics.

INTRODUCTION

Basal forebrain neurones provide the main cholinergic innervation to hippocampus and several cerebral cortical regions (Mesulam, Elliott, Levey & Wainer, 1983; McKinney, Coyle & Hedreen, 1983). Their degeneration has been implicated in the pathophysiology associated with dementia in man (Coyle, Price & DeLong, 1983). Whilst there have been a number of *in vitro* studies of the membrane properties of neurones in the medial septum and diagonal band (see for example; López-Barneo, Alvarez de Toledo & Yarom, 1985; Nakajima, Nakajima, Obata, Carlson & Yamaguchi, 1985; Griffith & Matthews, 1986; Griffith, 1988; Alvarez de Toledo & López-Barneo, 1988; Castellano & López-Barneo, 1991; Matthews & Lee, 1991), there is still little information regarding the types and properties of voltage-activated calcium currents expressed by these neurones (Castellano & Lopez-Barneo, 1991). The influx of calcium (Ca^{2+}) through voltage-gated channels is of crucial importance as it seems likely to contribute to the excitable behaviour of these neurones (Segal, 1986; Griffith, 1988; Alvarez de Toledo & López-Barneo, 1988), and might contribute to the process of neurodegeneration (Choi, 1988; Dreyer, Kaiser, Offermann & Lipton, 1990). Furthermore, cortical tissue from patients with Alzheimer's disease shows impaired synthesis and release of acetylcholine (Sims, Bowen, Allen, Smith, Neary, Thomas & Davison, 1983), presumably in terminals of basal forebrain neurones. Hence, information about the somatic Ca^{2+} currents in these cholinergic basal forebrain neurones might provide some insight into the regulation of transmitter release from their terminals, which could be of prospective value to understanding and correction of this deficit.

Accordingly, in the present paper we have studied some of the kinetic and pharmacological properties of somatic Ca^{2+} currents in dissociated, identifiably

cholinergic magnocellular basal forebrain neurones. The results reveal that these neurones express both low- and high-voltage-activated Ca^{2+} currents which display certain differences from those previously described in other central neurones (see Scott, Pearson & Dolphin, 1991 for review).

METHODS

Tissue preparation and acute dissociation

Acutely dissociated cell cultures of post-natal rat basal forebrain neurones were prepared using a combination of enzymatic and mechanical dissociation procedures. Sprague–Dawley rat pups (11–14 days old, weight range 29–32 g) were killed with an excess of chloroform, decapitated and the brain quickly removed and hemisected in cold dissecting medium, containing Gey's balanced salt solution (GBSS), supplemented with an additional 0·6% D-glucose, 8 mM $MgCl_2$ and 1 mM kynurenic acid. Coronal slices (400 μm thick) were cut using a McIlwain tissue chopper, collected in cold dissecting medium and regions of basal forebrain nuclei (namely, vertical and horizontal limbs of the diagonal band of Broca, substantia innominata, nucleus basalis and globus pallidus) were dissected out. The tissue fragments were incubated at 37 °C in Ca^{2+}-, Mg^{2+}-free Hank's balanced salt solution (HBSS), containing 0·125% trypsin for 45 min, then washed repeatedly in Ca^{2+}-free HBSS containing 8 mM $MgCl_2$, 10% fetal calf serum, 10 mg ml^{-1} ovomucoid and 0·01 mg ml^{-1} DNase I. The tissue was then mechanically dissociated in Ca^{2+}-free HBSS supplemented with 8 mM $MgCl_2$ and 0·02 mg ml^{-1} DNase I. The cell suspension was centrifuged at 27 *g* for 10 min and the pellet resuspended in 1 ml of growth medium of the following composition: Dulbecco's modified Eagle's medium (DMEM, 45%), Leibovitz L-15 (45%), L-glutamine (0·29 mg ml^{-1}), D-glucose (6 mg ml^{-1}), $NaHCO_3$ (3·3 mg ml^{-1}), heat-inactivated fetal calf serum (10%) and 7S-mouse nerve growth factor (25 ng ml^{-1}). The cells were plated out onto poly-D-lysine (0·05 mg ml^{-1})-coated 35 mm culture dishes (Cell-Cult), at a seeding density of 2×10^3 cells per dish. This dissociation procedure yielded cells with some of their processes intact, and following overnight plating at 37 °C in an atmosphere of 5% CO_2 in air, the processes retracted resulting in 'rounded' cells, which were well suited for voltage clamping, as problems with space clamp and synaptic connections are largely avoided. This semi-acute approach to isolating single cells from the postnatal mammalian central nervous system also has the additional advantage over the widely used acute enzymatic treatment of Kay & Wong (1986) in that the cells have time to recover from the enzymatic and mechanical treatment.

In a separate series of experiments, the cultures were stained for acetylcholinesterase (AChE), a cholinergic marker as described by Hedreen, Bacon & Price (1985) and counter-stained with Methylene Blue. Out of a population of 312 cells with somal diameters ranging from 20–38 μm, 93 $\pm$ 2% ($n = 6$ separate animal cultures) stained positive for AChE.

Electrophysiological studies

The dissociated cultures of basal forebrain neurones were routinely used after a period of 10–14 h incubation. The experiments were performed at room temperature (22–25 °C). The culture dishes were mounted onto the stage of an inverted microscope equipped with phase contrast optics (Nikon TMS) and superfused at a rate of 8–10 ml min^{-1} with 'normal' Krebs solution of the following composition (mM): NaCl, 118; KCl, 3; $MgCl_2$, 1·2; $CaCl_2$, 2·5; $NaHCO_3$, 25; HEPES, 5; D-glucose, 11, adjusted to pH 7·4 (where necessary) and gassed with 95% O_2–5% CO_2. Patch electrodes were made from borosilicate glass capillaries (1·5 mm diameter; Clark Electromedical Instruments). In order to reduce transluminal capacitance the tips of the electrodes were coated to within 100 μm of the tip with Sylgard (Dow Corning) and their tips fire-polished using a microforge (Nikon MF-9). The electrodes had resistances of 5–8 MΩ when filled with a caesium-containing internal solution of the following composition (mM): caesium acetate, 102·4; CsCl, 10·6; $MgCl_2$, 1; TEA-Cl, 5; HEPES, 40; ethylene glycol bis-(β-aminoethyl ether)*N*,*N*,*N*′,*N*′-tetraacetic acid (EGTA), 3; MgATP, 4; Na_2GTP, 0·1: The solution was adjusted to pH 7·25 with NaOH, and had a final osmolarity of 288 mosmol l^{-1}. The free calcium concentration was calculated and adjusted to 30 nM using the method of Portzehl, Caldwell & Rüegg (1964). Macroscopic currents through voltage-activated calcium (Ca^{2+}) channels were recorded using the whole-cell configuration of the patch-clamp technique (Hamill, Marty, Neher, Sakmann & Sigworth, 1981). After rupture of the gigaseal

cells were then voltage clamped using a discontinuous single-electrode voltage-clamp amplifier (Axoclamp-2), operated at a sampling rate of 7–15 kHz (30% duty cycle). Capacitance neutralization, gain and phase controls were adjusted to produce optimal clamp efficiency. Under these conditions, a clamp gain of between 0·7 and 2·5 nA mV^{-1} could be achieved. In a typical cell, this resulted in a clamp error, measured at the peak of the calcium current (step to 0 mV from V_H −80 mV) of ⩽ 3%. The reference electrode was a glass bridge containing 4% agar–saline, of which one end was placed in the culture dish and the other in a 3 M KCl side chamber connected to ground, via an Ag–AgCl pellet. Having established stable recording conditions the superfusing 'normal' Krebs solution was switched to one containing (mM): tetraethylammonium chloride (TEA-Cl), 30; NaCl, 91; $MgCl_2$, 1·2; $CaCl_2$, 2·5; $NaHCO_3$, 25; HEPES, 5; D-glucose, 11. In addition, 0·5 μM tetrodotoxin (TTX) was added to block inward sodium (Na^+) currents.

Data acquisition and analysis

Voltage command pulses were simultaneously generated and sampled on-line using a labmaster DMA interface (Axon Instruments) connected to an IBM PC/AT clone (Ness PC-286 S) computer. Signals were filtered at 0·3 or 1 kHz prior to digitizing using an in-built filter on the recording amplifier. Acquisition and subsequent analysis of the acquired data was carried out using the 'pClamp' suite of software (Axon Instruments). In addition, current and voltage signals were also recorded simultaneously onto a chart recorder (Gould 2400S). Curve fitting procedures were carried out using 'Graphpad' computer software (Graphpad, CA, USA). All data are expressed as means ± S.E.M.

Drugs

All drugs were bath-applied in the superfusing Krebs solution. Concentrated stock solutions of dihydropyridines (DHP) and diphenylalkyamine compounds, namely nifedipine (Sigma), nimodipine (gift from Bayer UK), nitrendipine (gift from Bayer UK), nicardipine (Sigma) and Bay K 8644 (Calbiochem) were prepared by dissolving the drug in tissue culture-quality dimethylsulphoxide (DMSO) and stored as aliquots at −20 °C. Working solutions were prepared just prior to use, by diluting the stock in superfusate resulting in a maximum final concentration of DMSO of 0·7% which on its own had no effect upon the calcium current in these cells. All experiments using DHPs were performed in a darkened room. Because the DHPs are very hydrophobic, the perfusion chamber and tubing were washed extensively with 20 ml of absolute alcohol after each cell and before setting up a new dish of culture. ω-Conotoxin fraction GVIA (initially as a gift from Dr A. Cross, Astra, and then from Peninsula Laboratories) were stored in HEPES–EGTA buffer (pH 7·4) as aliquots of 10 μM at −20 °C. Inorganic compounds, namely the chloride salts of calcium ($CaCl_2$), cadmium ($CdCl_2$), cobalt ($CoCl_2$), lanthanum ($LaCl_3$) and nickel ($NiCl_2$) were obtained from BDH and that of gadolinium ($GdCl_3$) from Aldrich.

RESULTS

Gigaseal formation and the establishment of whole-cell recording conditions were made whilst cells were being superfused with a standard, TEA-free, Krebs solution (see Methods). Resting membrane potentials measured immediately following patch rupture ranged between −65 and −80 mV. The health of each neurone was checked by evoking action potentials using intrasomal current injection. Only cells with an action potential amplitude of greater than 100 mV were used. Cells to be studied were then voltage clamped at −80 mV and the superfusing Krebs solution switched to one containing 30 mM TEA and 0·5 μM TTX. Inhibition of outward currents was monitored by imposing 0·5 s duration voltage steps to 0 mV every 2 min until the calcium current (I_{Ca}) reached a constant amplitude. This typically took between 5 and 15 min after which time the slope resistance of cells measured outside the activation range of I_{Ca} (−90 to −60 mV) or in the presence of 200 μM cadmium ranged between 0·27 and 2·77 GΩ (mean 1·13 ± 0·11 GΩ, $n = 37$). Under these

conditions, large inward Ca^{2+} currents could be recorded for at least 30 min without significant run-down.

Current–voltage relationship

Current–voltage (*I–V*) curves were constructed from a holding potential (V_H) of −80 mV. At this potential there was no steady-state inactivation of I_{Ca} (see Fig. 4). Depolarizing steps from V_H initially revealed a transient low-voltage-activated (LVA) current with a threshold between −60 and −47 mV (mean −54·4 ± 0·72 mV, $n = 19$; Fig. 1). Larger depolarizing steps recruited an additional high-voltage-activated (HVA) current with a threshold between −46 and −30 mV (mean

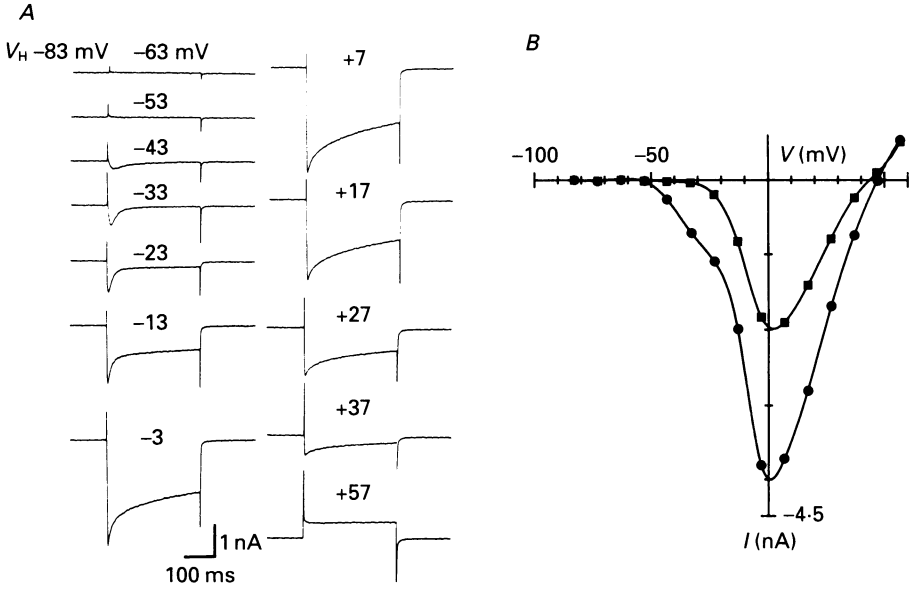

Fig. 1. Whole-cell calcium currents recorded from an isolated rat magnocellular cholinergic basal forebrain neurone in 2·5 mM extracellular calcium. *A*, examples of currents recorded on depolarizing from a holding potential (V_H) of −83 mV to the test potentials indicated for 300 ms. *B*, current–voltage (*I–V*) curves for the cell shown in *A*. ●, the peak current amplitudes; ■, amplitudes measured at the end of the depolarizing pulses. Current values have been plotted after subtraction of the holding current (−90 pA) but no correction has been made for leak.

−36·8 ± 1·9 mV, $n = 18$; Fig. 1). The amplitude of the HVA component of I_{Ca} increased steeply from threshold to reach a peak at command potentials between −6 and +6 mV (mean +0·36 ± 3·23 mV, $n = 21$), then declined with further depolarization with a null potential between +40 and +60 mV (Fig. 1*B*).

Calcium dependence

Under 'normal' conditions with 2·5 mM external calcium as the charge carrier (30 nM internal calcium) the peak of the calcium current in basal forebrain neurones ranged between 1 and 4 nA (mean 2·19 ± 0·068 nA. $n = 103$). Removal of extracellular Ca^{2+} and replacement with equimolar Mg^{2+} totally abolished all components of the calcium current. Figure 2*A* shows peak *I–V* curves constructed in various concentrations of $[Ca^{2+}]_o$. Raising $[Ca^{2+}]_o$ increased the amplitude of I_{Ca}, with a 10-

fold increase in $[Ca^{2+}]_o$ producing a positive shift of around 13 mV in the peak of the calcium current. This voltage shift was most probably caused by a change in the surface negative charge around the Ca^{2+} channels (Ohmori & Yoshii, 1977). Over the range of $[Ca^{2+}]_o$ tested (0·25–10 mM) the peak amplitude of the calcium current showed an approximately hyperbolic relationship to $[Ca^{2+}]_o$ with half-saturation at 2·5 mM (Fig. 2*B*).

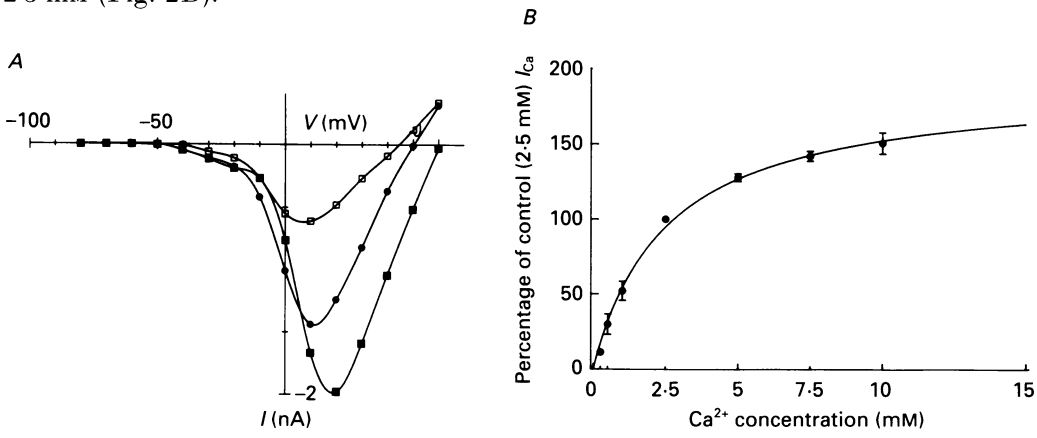

Fig. 2. Calcium dependence of I_{Ca} in magnocellular rat basal forebrain neurones. *A*, *I–V* curves of peak I_{Ca} in 1 (□), 2·5 (●) and 10 mM (■) extracellular calcium respectively. Increasing extracellular Ca^{2+} ($[Ca^{2+}]_o$) shifted the peak of the calcium current to more positive potentials, with approximately a 13 mV shift for a 10-fold increase in $[Ca^{2+}]_o$. *B*, dependence of the peak amplitude of the I_{Ca} on $[Ca^{2+}]_o$. Currents were evoked by stepping from a holding potential of −80 mV to 0 mV for 300 ms. Ordinate shows I_{Ca} expressed as percentage of that recorded in 2·5 mM Ca^{2+}. The curve has been fitted using non-linear regression, according to the equation $I_{Ca} = I_{Ca(max)} \{[Ca^{2+}]_o/([Ca^{2+}]_o + K_{Ca})\}$ where the half-saturation concentration (K_{Ca}) = 2·5 mM and $I_{Ca(max)}$ = 190·6 % (correlation coefficient $r^2 = 0{\cdot}996$).

Transient LVA current

The presence of the LVA current resulted in a small hump in the *I–V* curve between −50 and −25 mV (V_H −80 mV). The amplitude of the LVA component of I_{Ca} ranged between 0·15 and 1·32 nA, and was generally less than 20% of the amplitude of the peak whole-cell current measured at 0 mV (range 3·8–47·3 %; mean 16·5 ± 2·1 %, $n = 19$). Hyperpolarizing pre-pulses to −120 mV for 100–500 ms (V_H −80 mV) prior to jumping to −25 mV were never observed to remove any steady-state inactivation of the LVA current ($n = 4$). The voltage dependence of activation and inactivation of the transient LVA current was therefore examined from a holding potential of −80 mV using the protocol shown in Fig. 3*A*. The rate and degree of activation of the LVA current were both strongly voltage dependent. The average time-to-peak (t_p) decreased with depolarization from a mean value of 39·1 ± 2·3 ms at −50 mV to 6·4 ± 0·6 ms at −20 mV ($n = 16$; Fig. 3*A* and *D*). The t_p decreased exponentially with membrane depolarization, with an e-fold change for a 16·1 mV change in command potential. The amplitude of the LVA current increased steeply with depolarization, reaching a peak at between −10 and −20 mV. The activation curve could be fitted with a Boltzmann equation of the form:

$$I/I_{max} = 1/\{1 + \exp[(V - V_{\frac{1}{2}})/k]\},$$

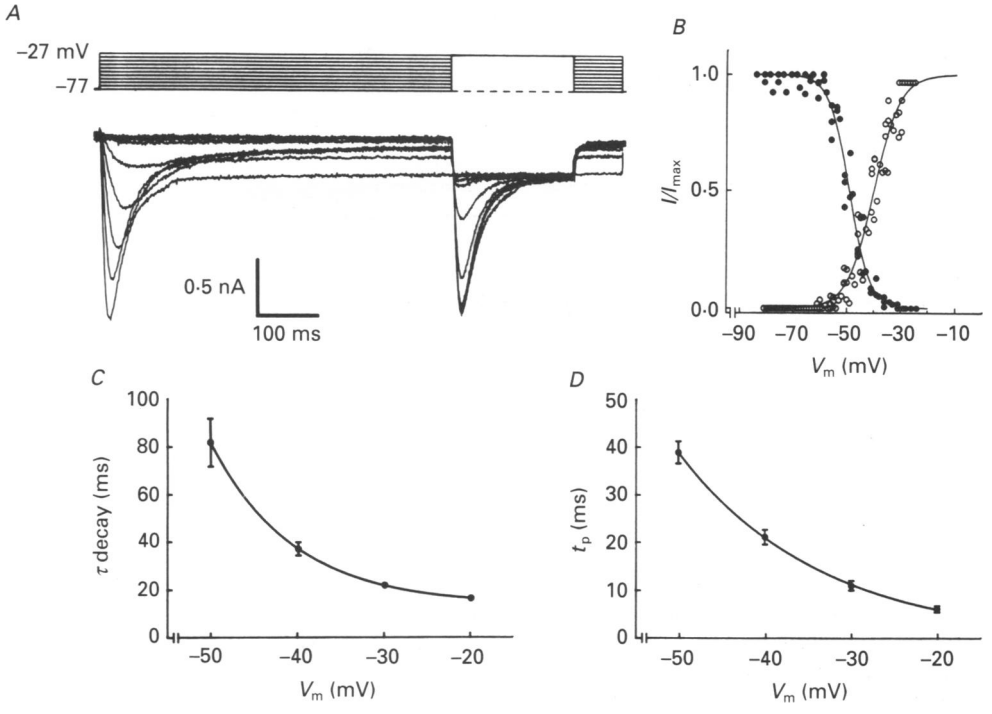

Fig. 3. Kinetics of the transient low-voltage-activated current (LVA) in basal forebrain neurones. *A*, an example of the protocol used to investigate the voltage dependence of activation and inactivation of the LVA component of I_{Ca}. The individual traces have been corrected for leak current recorded in the presence of 200 μM Cd^{2+}. The protocol was designed to enable activation and inactivation to be examined concurrently in the same cell. Cells were nominally held at a V_H of −80 mV (−77 mV in this example). Activation of the LVA current was investigated by imposing a series of increasing amplitude depolarizing steps (500 ms duration, 5 mV increments); at the end of each of these depolarizing steps the cell was then commanded to a nominal potential of −30 mV for 200 ms in order to study the steady-state voltage dependence of inactivation. Between individual episodes the cell was held at −80 mV for 30 s. *B* shows activation (○) and inactivation (●) curves constructed from data obtained as in *A*. The activation curve was constructed by normalizing the amplitude of the LVA current with respect to the current evoked at −30 mV and plotting these values against command potential. The data from nine cells were pooled and fitted by non-linear regression to a Boltzmann equation (see text; $r^2 = 0{\cdot}967$) where only the minimum value (0) was constrained. This yielded a theoretical I_{max} to which all the activation data were then re-normalized before plotting. The extrapolated peak activation of the LVA current was between −10 and −20 mV, with a half-activation potential of −40·2 mV and a slope value (k) of 4·8 mV. Data for the inactivation curve were pooled from five cells where the data had been normalized with respect to the value obtained on stepping from −80 to −30 mV. This was then fitted by non-linear regression to a Boltzmann equation ($r^2 = 0{\cdot}980$) which yielded a half-inactivation potential of −49·3 mV and a slope value (k) of 3·8 mV. *C*, the time constant for decay (τ_{decay}) of the LVA current at different test potentials (V_H −80 mV). Each point is the mean ± S.E.M. of twelve to sixteen cells. The points were fitted to an equation of the form $A\ e^{-kt} + C$. The continuous line ($r^2 = 1{\cdot}000$) indicates exponential voltage dependence of τ_{decay} with an e-fold change for a 9·6 mV change in V_m and a theoretical minimum of 12·8 ms. *D*, the time to peak (t_p) of the LVA current at different test potentials (V_H −80 mV). Each point is the mean ± S.E.M. of sixteen cells. The t_p decreased exponentially ($r^2 = 1{\cdot}000$) with an e-fold acceleration per 16·1 mV change in V_m.

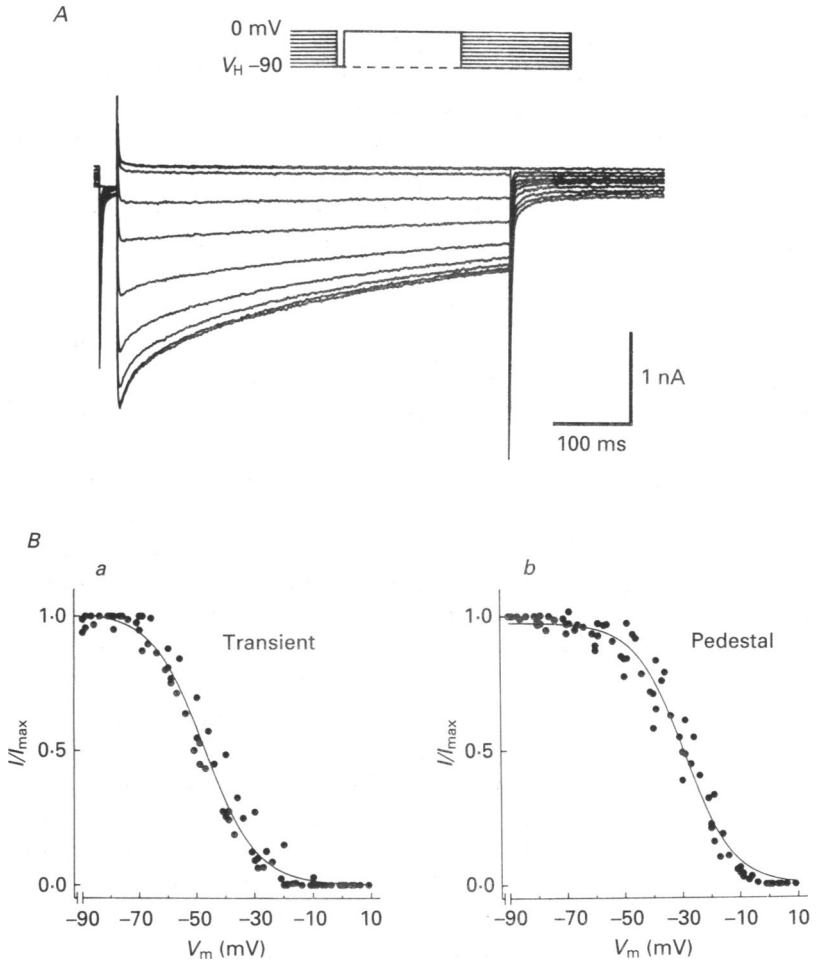

Fig. 4. Voltage-dependent inactivation of the decaying (transient) and sustained (pedestal) components of HVA current in rat basal forebrain neurones. *A*, a typical series of current records showing the degree of inactivation of I_{Ca} at different test potentials. Control currents were elicited by stepping to 0 mV for 500 ms from a holding potential (V_H) of −90 mV. Inactivation of the current was studied by imposing a series of increasing amplitude depolarizing pre-pulses of 60 s duration (10 mV increments) prior to stepping to 0 mV. An additional step back to −90 mV for 20 ms was imposed immediately prior to jumping to 0 mV in order to allow gating charges to be returned to their deactivated state. Examination of the current traces shown in panel *A* reveals that the calcium current did not reach a sustained value within 500 ms. Therefore, in order to obtain a more accurate assessment of the amplitudes of the transient and 'true sustained' (pedestal) components of the calcium current, their contributions were measured by curve fitting. The decay phase of the calcium current was usually best fitted by two exponential functions. The contribution played by this transient current was calculated by extrapolation to the point at which these two decaying components had declined by > 99·9%, whilst the 'true' sustained (pedestal) was calculated as peak minus total transient current. (Note: in a few cells, a good fit of the decay phase of the current required three exponential functions. In these cells, the additional exponential had a τ value of 9–14 ms and was sensitive to low concentrations of Ni^{2+} indicating that it was due to residual LVA current (see text). In such cases the amplitude of this component was not included in the

with a half-activation potential ($V_{\frac{1}{2}act}$) of −40·2 mV and a slope factor (k) of 4·8 mV (Fig. 3*B*).

The LVA current inactivated mono-exponentially. The rate of inactivation was voltage dependent: the mean value for the decay time constant (τ_{decay}) decreased from 81·7 ± 9·9 ms (n = 12) at −50 mV to 15·7 ± 0·9 ms at −20 mV (n = 16; Fig. 3*A* and *C*). Inactivation rate was exponentially related to membrane potential, with an e-fold change in τ_{decay} for a 9·6 mV change in the test potential. Steady-state inactivation could be fitted with a Boltzmann equation, with a half-inactivation potential ($V_{\frac{1}{2}inact}$) of −49·3 mV and slope factor (k) of 3·8 mV (n = 5; Fig. 3*B*).

HVA current

The HVA current exhibited both decaying (transient) and sustained components. In general, the decaying phase of the calcium current elicited at 0 mV was best fitted by two exponential functions with time constants τ_{fast} = 16·2 ± 2·5 ms and τ_{slow} = 301·3 ± 22·7 ms (n = 17). These two kinetically distinct transient components of the current accounted for 16·1 ± 2·2 and 45·4 ± 2·3 % of the peak calcium current at 0 mV respectively, with the remaining 39·5 ± 1·7 % being carried by an extrapolated sustained 'pedestal' current. In a few cells, the decaying phase of the calcium current involves an additional rapidly inactivating component. Two factors indicate that this was carried by residual T-type LVA current. Firstly, the time constant of decay of this component (9–14 ms) was similar to that which would be predicted for the LVA current at this potential (see above and Fig. 3*C*). Secondly, its amplitude was reduced by low concentrations of Ni^{2+} (5–10 μM) and amiloride (50–300 μM) which were selective for the T-type LVA current in these cells (see later and Fig. 6).

The voltage dependence of inactivation of the HVA current was studied using the pre-pulse protocol shown in Fig. 4*A*. In the present study, Ca^{2+} as the physiological charge carrier was deliberately chosen in preference to the more conventional carrier Ba^{2+}. Therefore, we cannot exclude the possibility that part of the observed inactivation process results from Ca^{2+}-dependent rather than voltage-dependent inactivation. Inactivation of the transient component could be fitted with a Boltzmann equation with $V_{\frac{1}{2}inact}$ of −47·3 mV and slope factor k of 9·04 mV (Fig. 4*Ba*). Corresponding values for the pedestal current were −29·2 and 11·8 mV respectively (Fig. 4*Bb*).

Pharmacology of the calcium current

Conotoxin

ω-Conotoxin GVIA (ω-CgTX; 100 nM) has been reported to inhibit a component of HVA Ca^{2+} current in a variety of peripheral and central neurones (see Sher & Clementi, 1991, for review). Figure 5 illustrates the principal effects of ω-CgTX on I_{Ca}

amplitude of the transient HVA current.) *Ba* and *b* show the inactivation curves for the transient and pedestal components of the HVA current as described above, constructed in each case from data pooled from eight cells. The data in *Ba* and *b* were fitted using non-linear regression to a Boltzmann equation (see text). This yielded values for the half-inactivation potential ($V_{\frac{1}{2}}$), and slope (k) for the transient and pedestal components of the HVA current of −47·3 mV and 9·04 (r^2 = 0·984) and −29·2 mV and 11·8 (r^2 = 0·978) respectively.

on basal forebrain neurones. At 100 nM ω-CgTX produced a slowly developing partial block of the HVA current, which was maximal after 4–6 min perfusion (Fig. 5*A*) and no additional reduction in I_{Ca} could be obtained by increasing the concentration up to 500 nM. No wash-out of the block was observed over a 20 min period and thus

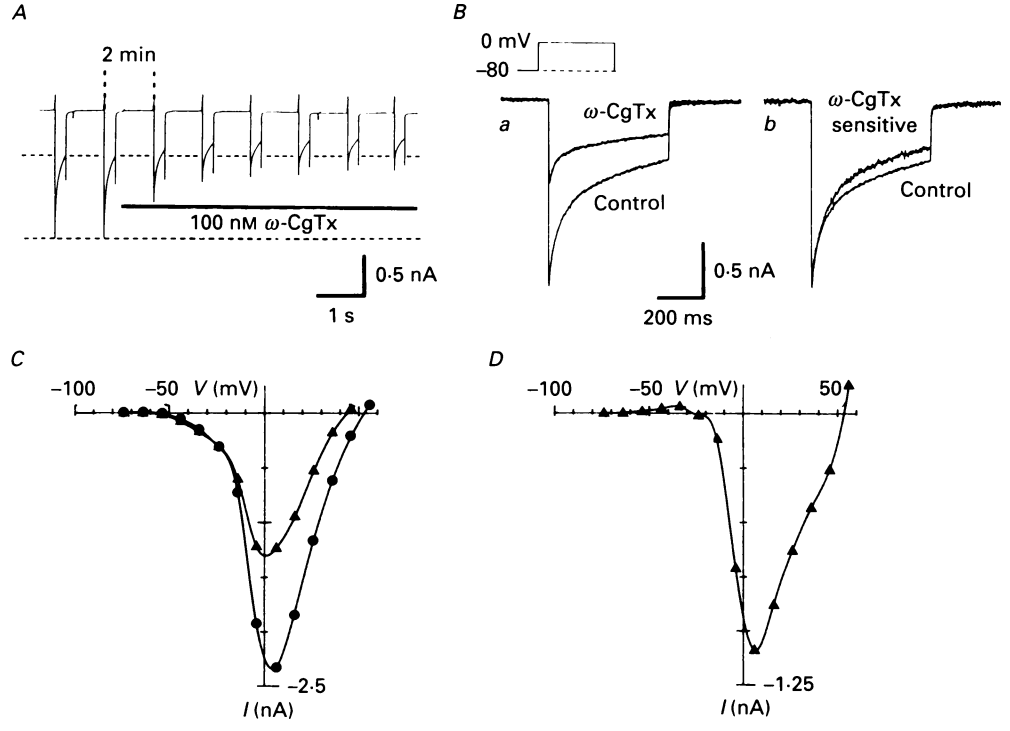

Fig. 5. The action of ω-conotoxin (ω-CgTX) on the calcium current (I_{Ca}) in rat basal forebrain neurones. *A*, time course of block by 100 nM ω-CgTX. The cell was held at −80 mV and stepped to 0 mV for 500 ms once every 2 min. The speed of the chart recorder was increased 100-fold for a brief period before, during and after (total 1 s) each command to 0 mV. *Ba*, currents recorded from the cell shown in *A* after leak subtraction using leak currents obtained in the presence of 200 μM Cd^{2+}, in the absence and presence of 100 nM ω-CgTX. *Bb*, comparison of the decay kinetics of the control and ω-CgTX-sensitive components of I_{Ca}. The ω-CgTX-sensitive current was obtained by digitally subtracting the two traces shown in *Ba*. The peak of the ω-CgTX-sensitive current has been normalized with respect to that of the control. The ω-CgTX-sensitive current in this (and all other cells studied) peaked rapidly then decayed during the course of the 500 ms command pulse. *C*, the peak current *I–V* relationship for a second cell under control conditions (●) and at equilibrium in the presence of 100 nM ω-CgTX (▲). ω-CgTX had almost no effect upon the LVA component of I_{Ca}, which reveals itself as a hump in the *I–V* curve at potentials between −55 and −15 mV. It did, however, have a marked blocking effect on HVA current at more depolarized potentials, resulting in a small shift in the peak of the composite *I–V* relationship to more hyperpolarized potentials (≈ 8 mV). *D*, an *I–V* plot of the digitally subtracted ω-CgTX-sensitive current for the cell shown in *C*.

inhibition was essentially irreversible. Block was restricted to the HVA component of current activated at potentials ⩾ 20 mV, with no significant effect on the transient LVA current (Fig. 5*C*). The component of HVA current inhibited by ω-CgTX could

not be separated from the remaining current in terms of its activation range (Fig. 5*C* and *D*). However, inspection of the current in the absence and presence of ω-CgTX revealed some change in kinetics (Fig. 5*Ba*), such that the ω-CgTX-sensitive component showed a more pronounced decay during the command step (Fig. 5*Bb*).

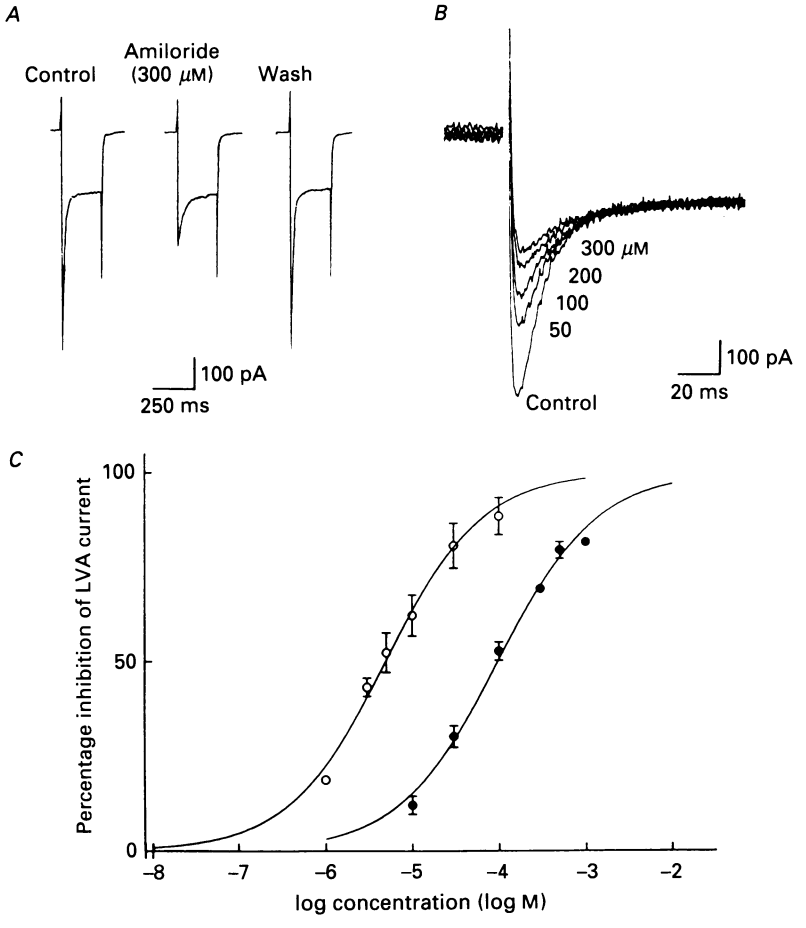

Fig. 6. Inhibition of the low-voltage-activated (LVA) component of the whole-cell current by amiloride and nickel. *A*, selective and reversible partial inhibition of the LVA current by amiloride (300 μM). Currents were evoked using 250 ms commands to −30 mV from a holding potential of −80 mV. *B*, concentration dependence of the block by amiloride (50–300 μM) on the initial transient LVA component of the calcium current. Data from the same cell as shown in *A* but on a faster time base. *C*, dose–response curves for amiloride (●) and Ni^{2+} (○) yielded IC_{50} values of 97 and 5 μM respectively (all data points are the means ± S.E.M. of 3–7 cells).

Notwithstanding, ω-CgTX did not eliminate either of the two kinetically separable components of current decay described earlier: the time course of ω-CgTX-sensitive current still showed two components of decay, with time constants τ_1 of 19·8 ± 3·8 ms and τ_2 of 244·1 ± 21·6 ms which contributed 18·7 ± 2·65 and 54·9 ± 3·64% ($n = 18$) respectively of the total peak ω-CgTX-sensitive current at 0 mV.

Amiloride

Amiloride has previously been shown to block T-type LVA calcium currents in both peripheral and central neurones (Bean, 1989; Scott *et al.* 1991). Figure 6*A* and *B* illustrates the effects of amiloride on the LVA component of I_{Ca} at −30 mV.

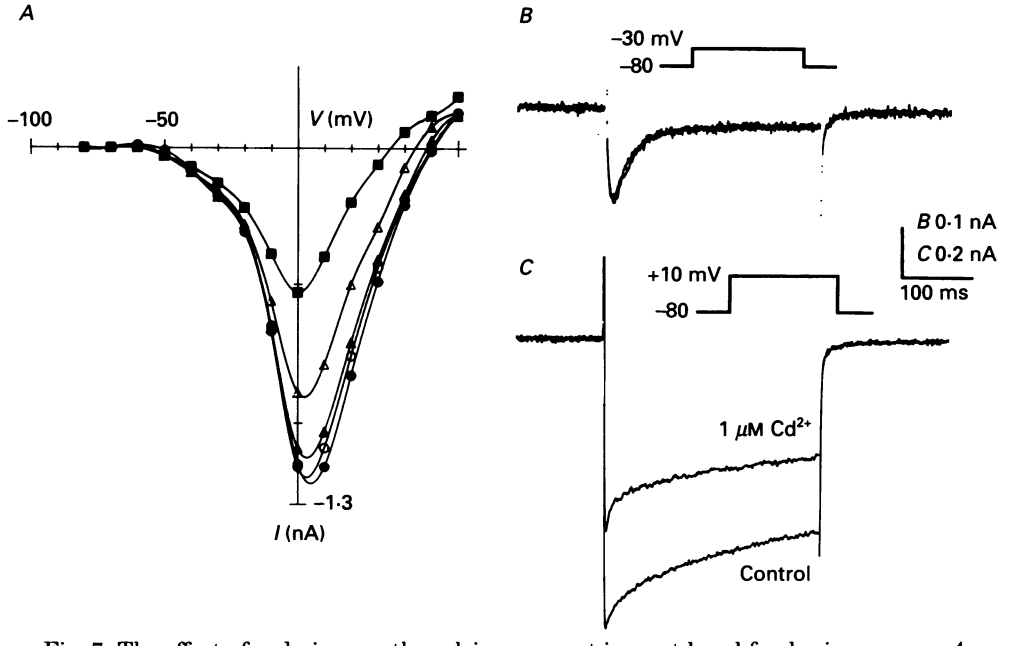

Fig. 7. The effect of cadmium on the calcium current in a rat basal forebrain neurone. *A*, peak *I–V* curves (300 ms duration steps every 30 s) under control (●) conditions and in the presence of increasing concentrations of Cd^{2+} (○, 0·1 μM; ▲, 0·3 μM; △, 1 μM; ■, 3 μM). At concentrations ⩽ 1 μM Cd^{2+} had no effect upon the LVA component of the current at command potentials negative to −20 mV. *B* and *C*, calcium currents from the cell shown in *A*, evoked by stepping from V_H to −30 and +10 mV respectively in the presence and absence of 1 μM Cd^{2+}. The transient LVA current, unlike the HVA current, was resistant to 1 μM Cd^{2+}.

Amiloride (50–300 μM) produced a dose-dependent block of the transient LVA component of I_{Ca} (IC_{50} = 97 μM; see Fig. 6*B* and *C*). At concentrations ⩽ 300 μM amiloride produced a readily reversible and selective partial block of the transient LVA current with little or no effect upon the component of HVA current activated at −30 mV (Fig. 6*A* and *B*). At concentrations > 300 μM, amiloride inhibited more of the T-type LVA current but was no longer selective and caused depression of both the peak and sustained components of HVA current.

Block of I_{Ca} by inorganic ions

Divalent cations

Nickel has been reported to preferentially block LVA current whereas cadmium preferentially blocks HVA current (for review see Scott *et al.* 1991). Similar effects were also seen in basal forebrain neurones. Figure 7*A* shows the effect of increasing

concentrations of Cd^{2+} (0·1–3 μM) on the peak current *I–V* relationship. From this it can be seen that at low concentrations ($\leqslant 1$ μM) Cd^{2+} markedly inhibited I_{Ca} at depolarized test potentials (more positive than −20 mV), but had little or no effect upon the LVA current. This selectivity could be most clearly observed when the cell

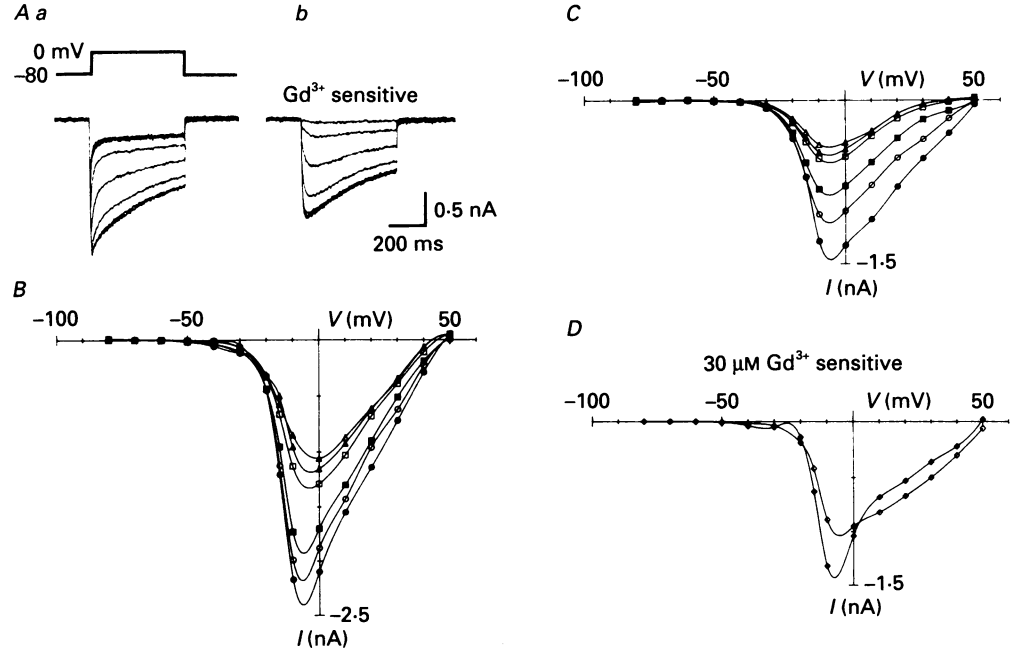

Fig. 8. Block of the calcium current (I_{Ca}) by the lanthanide ion gadolinium (Gd^{3+}). *Aa*, the effect of increasing concentrations of Gd^{3+} (0·1–100 μM) on the whole-cell calcium current evoked by stepping to 0 mV for 500 ms from a holding potential (V_H) of −80 mV. The block by Gd^{3+} increased in a dose-dependent manner, before reaching a maximum at concentrations between 30 and 100 μM. Currents have been leak-subtracted by subtracting the current recorded in 200 μM Cd^{2+}. *Ab*, the digitally subtracted Gd^{3+}-sensitive currents for the cell shown in *Aa*. The time-to-peak of the Gd^{3+}-sensitive current decreased with increasing concentrations of Gd^{3+}. The current then decayed mono-exponentially from this initial peak during the course of the step. *B* and *C*, peak (*B*) and sustained (*C*) *I–V* curves constructed under control conditions (●) and in the presence of 1 (○), 3 (■), 10 (□) 30 (▲) and 100 μM (△) Gd^{3+}. Gd^{3+} had little effect at hyperpolarized membrane potentials (> −20 mV) but markedly reduced the amplitude of the currents positive to −20 mV. *D*, *I–V* curves of the peak (◆) and sustained (◇) Gd^{3+}-sensitive currents obtained by digital subtraction of current recorded in the absence and presence of 30 μM Gd^{3+}. The threshold and peak current values for the Gd^{3+}-sensitive current were similar for both the peak and sustained components of I_{Ca}, (approximately −25 mV for the threshold and −10 mV for the peak current respectively).

was clamped at −80 mV and stepped alternately to −30 mV (evoking primarily LVA current; Fig. 7*B*) and to +10 mV (recruiting HVA current; Fig. 7*C*). At higher concentrations (3–200 μM) this selectivity was lost and Cd^{2+} (3–200 μM) inhibited all components of I_{Ca} in a dose-dependent manner, with an IC_{50} value on both the sustained (see Fig. 10) and peak calcium currents of 2 μM.

In contrast to Cd^{2+}, Ni^{2+} more potently inhibited the transient LVA current than

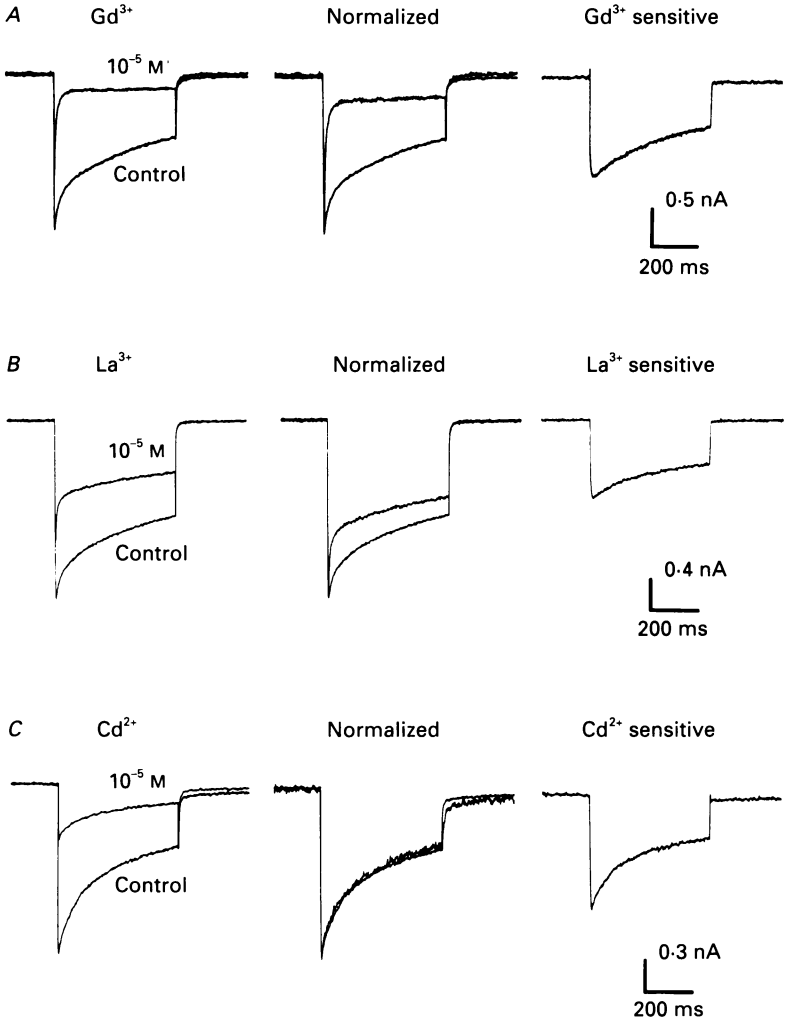

Fig. 9. The effects of Gd^{3+}, La^{3+} and Cd^{2+} ions (10 μM) on the decay kinetics of the whole-cell calcium current evoked by stepping to 0 mV for 500 ms from a holding potential of −80 mV. In *A*, *B* and *C*, the left-hand panel shows the calcium current under control conditions and in the presence of 10 μM Gd^{3+}, La^{3+} and Cd^{2+} respectively. The centre panels show currents recorded in the presence of the trivalent cations normalized with respect to the peak of the control and superimposed on the control current. The right-hand panels show the digitally subtracted Gd^{3+}-, La^{3+}- and Cd^{2+}-sensitive currents respectively. From these data, it can be seen that Gd^{3+} and La^{3+} both reduced the peak amplitude of the calcium current and markedly increased the initial rate of decay of the current. In contrast, Cd^{2+} blocked the current with little or no effect upon the decay kinetics of the residual current.

any other component of I_{Ca}. The IC_{50} against the LVA component was 5 μM (Fig. 6*C*), whereas for the sustained HVA current the IC_{50} value was 89 μM (Fig. 10). Notwithstanding, the overlap in the dose–response curves for the two components was still such that concentrations of Ni^{2+} required to totally block the LVA current (100 μM) inevitably produced some inhibition of the HVA current.

Trivalent cations

The sensitivity of I_{Ca} to two trivalent Ca^{2+} channel blockers, gadolinium (Gd^{3+}) and lanthanum (La^{3+}) was also investigated. Both of these ions produced a near maximal, incomplete, block of I_{Ca} at concentrations between 10 and 100 μM (Fig.

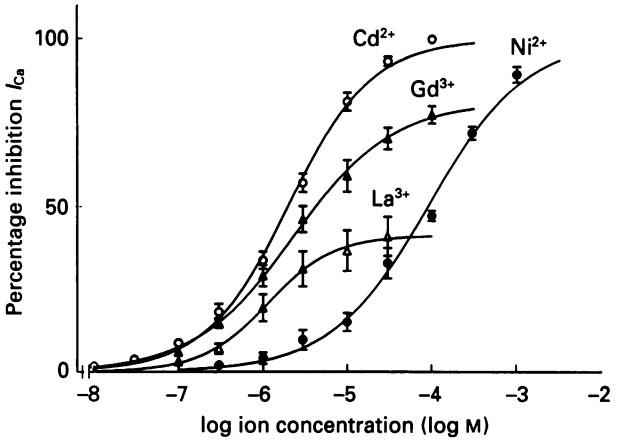

Fig. 10. Dose–response curves showing the effects of divalent and trivalent cations upon the sustained component of the HVA calcium current in magnocellular rat basal forebrain neurones. Calcium currents were elicited every 2 min by stepping to 0 mV for 500 ms from a holding potential of −80 mV. Dose–response curves were constructed by measuring the amplitude of the sustained component of the current at 500 ms, under control conditions and in the presence of increasing concentrations of the different cations. All data points are the means ± S.E.M. of four to eight cells. In each case data were fitted by non-linear regression to a hyperbolic curve. ○, Cd^{2+}, IC_{50} 2 μM, Hill slope 0·94; ▲, Gd^{3+}, IC_{50} 2·2 μM, slope 0·74; △, La^{3+}, IC_{50} 1·1 μM, slope 1·1; ●, Ni^{2+}, IC_{50} 89 μM, slope 0·75.

8*A a*). Examination of the peak and sustained (end of 500 ms step) *I–V* relationships for I_{Ca}, show that the block by Gd^{3+} was largely confined to HVA current activated at potentials more positive than −25 mV (Fig. 8*B* and *C*). The corresponding *I–V* relationships for the Gd^{3+}-sensitive current could not be distinguished from those of the control HVA current on the basis of either their activation or peak potentials (see Fig. 8*B–D*). A similar situation was also observed with La^{3+} (data not shown).

Neither trivalent ion blocked I_{Ca} as completely as Cd^{2+} (see Fig. 10); however, Gd^{3+} produced a much more complete block than La^{3+}. At a near maximally effective concentration, Gd^{3+} (100 μM) blocked 76·5 ± 2·6%, IC_{50} 2·2 μM ($n = 9$), of the sustained current (end of a 500 ms step to 0 mV) whereas a similarly effective dose of La^{3+} (30 μM) only inhibited 41·2 ± 5·9% of the current, IC_{50} of 1·1 μM ($n = 5$; Fig. 10).

Gd^{3+}, and to a lesser extent La^{3+}, produced a striking acceleration in the rate of decay of the HVA Ca^{2+} current, whereas Cd^{2+} did not affect the decay kinetics of the current (Fig. 9). As a result, the subtracted (trivalent cation-sensitive) components of current $I_{Ca(Gd)}$ and $I_{Ca(La)}$ had a rather unique trajectory, with a relatively slow time to peak, which accelerated with increasing ion concentration (Fig. 8*A b*), and had a similar mono-exponential decay ($\tau_{Gd} = 251·3 \pm 47·1$ ms, $n = 8$; $\tau_{La} = 241·1 \pm 49·8$ ms, $n = 4$).

This recalls the effect of Gd^{3+} on neuroblastoma cells described by Docherty (1988), which was interpreted to suggest that Gd^{3+} selectively inhibited a kinetically distinct component of I_{Ca}. The possibility that Gd^{3+} and La^{3+} might be selectively blocking a distinct component of I_{Ca} was examined further by studying their

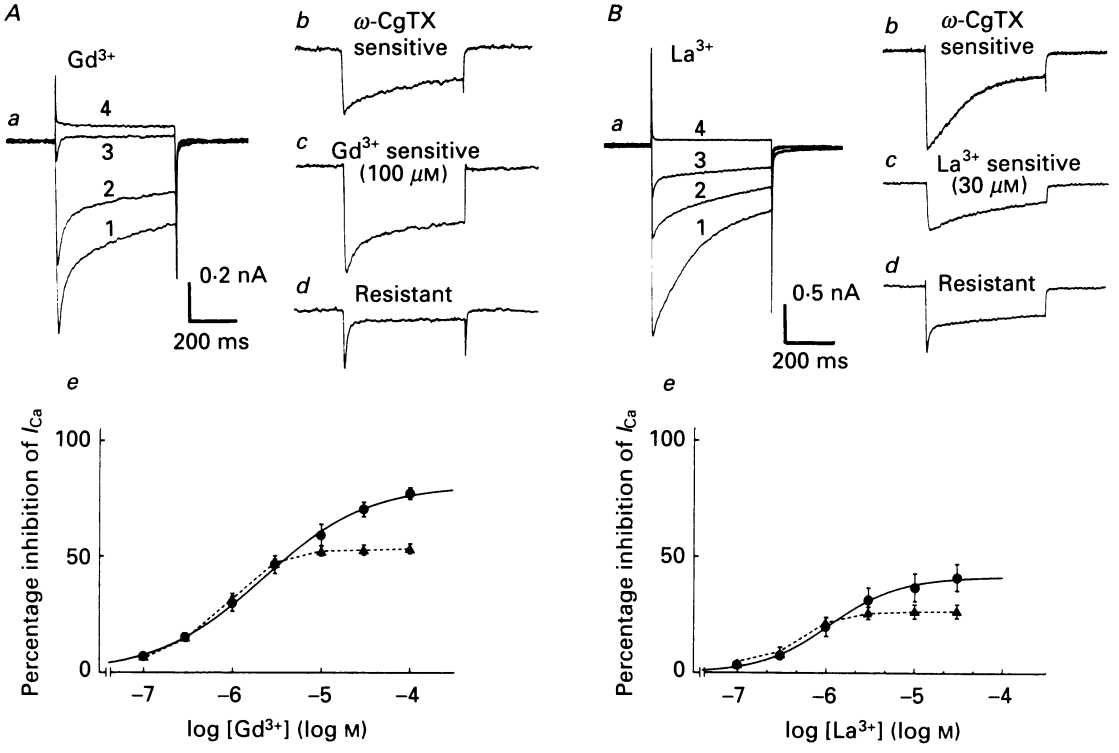

Fig. 11. The block of I_{Ca} by ω-CgTX, Gd^{3+} and La^{3+}. *Aa*, the combined actions of Gd^{3+} and ω-CgTX on the sustained calcium current (I_{Ca}) evoked by stepping from V_H (−80 mV) to 0 mV for 500 ms. Trace 1, control current; trace 2, after maximal block by ω-CgTX (100 nM); trace 3, after substituting the ω-CgTX, which produced an irreversible block, for Gd^{3+} (100 μM); trace 4, after adding 200 μM Cd^{2+}. *Ab*, *c* and *d* show the kinetics of the digitally subtracted ω-CgTX-sensitive, Gd^{3+}-sensitive and ω-CgTX/Gd^{3+}-resistant components of I_{Ca} respectively. *Ae*, dose–response curves to Gd^{3+} constructed under control conditions (●) and after maximal block by ω-CgTX (100 nM; ▲). In each case, the degree of block is expressed in terms of percentage inhibition of the initial control (pre-ω-CgTX) current. Data are the means ± S.E.M. of four to six cells. The control curve was fitted by non-linear regression to a sigmoid curve with a slope of 0·87 giving an IC_{50} value of 2·4 μM ($r^2 = 0{\cdot}9980$). A simple point-to-point dashed line was used to connect the individual data points for the dose–response relationship in the presence of ω-CgTX. These two curves show that the percentage inhibition of the initial control current produced by Gd^{3+} (≤ 3 μM) was unaffected by pre-treatment with ω-CgTX. Higher concentrations of Gd^{3+} (3–100 μM) produced a slight (≈ 20%) increase in degree of block. *Ba–e* shows data from identical experiments to those in *A* except that La^{3+} ions have been substituted for Gd^{3+} ions. Under control conditions, the IC_{50} value for La^{3+} was 1·1 μM and the Hill slope was 1·2. *Be* shows that like Gd^{3+}, La^{3+} at concentrations ≤ 1 μM is selective for a non-ω-CgTX-sensitive component of I_{Ca}.

pharmacological selectivity, in particular the block produced by these ions in the presence and absence of ω-CgTX (Fig. 11). The principal finding of these experiments was that at low concentrations (≤ 3 μM Gd^{3+}, ≤ 1 μM La^{3+}), trivalent cations and ω-

CgTX appeared to inhibit separate components of I_{Ca}. Thus, in the absence of ω-CgTX, Gd^{3+} blocked 43·9±3·9% ($n = 10$) of the sustained HVA current (end of 500 ms step to 0 mV; V_H −80 mV), whereas, when 36·8±2·0% of the total sustained current had been blocked by pre-treatment with 100 nM ω-CgTX, 3 μM Gd^{3+} still

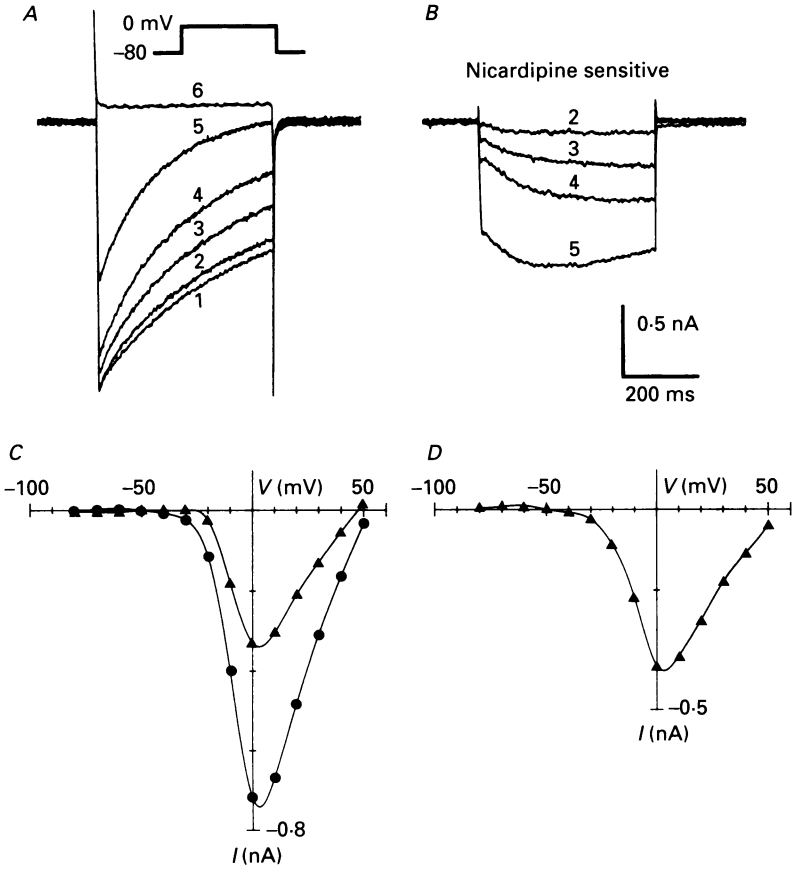

Fig. 12. The actions of the dihydropyridine antagonist nicardipine upon the whole-cell calcium current in magnocellular rat basal forebrain neurones. *A*, calcium currents evoked by jumping to 0 mV for 500 ms from a holding potential (V_H) of −80 mV under control conditions and in the presence of increasing concentrations of nicardipine. Trace 1, control; traces 2–5, in the presence of nicardipine at 1 (trace 2), 3 (trace 3), 10 (trace 4) and 30 μM (trace 5); trace 6, the evoked current in 200 μM Cd^{2+}. *B*, the digitally subtracted nicardipine-sensitive currents for the cell shown in *A*. At all concentrations the amplitude of the nicardipine-sensitive current increased during the voltage command and displayed little decay except at the highest concentration. The numbers beside each trace correspond to the concentrations of nicardipine given above for *A*. *C*, *I–V* plots of the sustained component of I_{Ca} (end of 300 ms step) under control conditions (●) and in the presence of 10 μM nicardipine (▲). I_{Ca} was evoked every 30 s from a holding potential of −80 mV. Nicardipine reduced the amplitude of the calcium current at all test potentials. *D*, the *I–V* relationship for the nicardipine-sensitive current (10 μM) for the cell shown in *C*. The threshold for the current was at approximately −40 mV and reached a peak at around 5 mV, like control current (see *C*).

blocked the same fraction (47·3 ± 1·3 %; $n = 4$) of the original (pre-ω-CgTX) current (Fig. 11*Ae*). Hence, block by ω-CgTX and Gd^{3+} summated rather than occluded. Essentially the same results were obtained using a combination of 1 μM La^{3+} and 100 μM ω-CgTX, with 19·5 ± 4·1 % ($n = 6$) of the current being inhibited before ω-CgTX and 21·3 ± 2·3 % ($n = 5$) after ω-CgTX (Fig. 11*Be*). With higher concentrations of trivalent cations, there was distinct overlap with the current blocked by ω-CgTX. Nevertheless, it is clear from these experiments that the trivalent cations and ω-CgTX preferentially inhibit separate components of HVA calcium current. In the case of Gd^{3+} and ω-CgTX, each component accounted for approximately 40 % of the total current so that, by combining the two, more than 80 % of the sustained HVA current could be blocked.

1,4-Dihydropyridines

The primary site of action for 1,4-dihydropyridine (DHP) compounds is believed to be on the L-type calcium channel (see Bean, 1989) although, recently they have also been reported to inhibit the T-type LVA current in some central and peripheral neurones (Akaike, Kostyuk & Osipchuk, 1989; Richard, Diochot, Nargeot, Baldy-Moulinier & Valmier, 1991). In the present study, we have attempted to evaluate the effects of a variety of DHP Ca^{2+} antagonists and agonists on both HVA and LVA component of the calcium current in magnocellular basal forebrain neurones. Figure 12 illustrates the principal effects of DHP Ca^{2+} antagonists, as typified by nicardipine, on the HVA component. Nicardipine (1–30 μM) produced a concentration-dependent increase in the degree of block, accompanied by an acceleration in the rate of decay of the current (Fig. 12*A*). The nicardipine-sensitive current had a slow rising phase and displayed little or no decline during the course of the voltage command (Fig. 12*B*). At sufficiently high concentrations (50–100 μM) nearly all of the sustained component of HVA current could be blocked by nicardipine (Fig. 13*A*). However, at these concentrations DHPs are near the limit of solubility in aqueous solution and thus these may not be the true bath concentrations. Dose–response curves were constructed to determine the relative potencies of the different DHP antagonists on the HVA current (Fig. 13*A*). In each case DHPs were applied cumulatively under low light conditions, allowing an equilibration period of 4–8 min at each concentration. At the end of each experiment Cd^{2+} (200 μM) was applied in order to obtain a value for the leak current. In rat basal forebrain neurones full wash-out of high concentrations of DHP compounds (especially nicardipine) was rarely possible, so a new culture was used for each attempted dose–response curve. The perfusion was also washed after each run with ethanol and distilled water to remove any DHPs bound to the tubing. Inhibition was measured as the percentage inhibition of the control (leak subtracted) sustained calcium current. This yielded a rank order of potency for inhibition of the HVA current of nicardipine > nitrendipine > nimodipine > nifedipine, with corresponding IC_{50} values of 6·9, 14·5, 60·8 and 203 μM respectively (Fig. 13*A*).

Equivalent concentrations to those which reduced the HVA current in basal forebrain neurones also inhibited the LVA current. Dose–response curves were constructed for the inhibition of the LVA current activated at −30 mV (V_H −80 mV) by the different DHP Ca^{2+} antagonists (Fig. 13*B*). The order of potency was nicardipine > nitrendipine = nimodipine > nifedipine and the apparent IC_{50}

values were 0·77 μM (nicardipine), 8·2 μM (nitrendipine and nimodipine) and 97·5 μM (nifedipine). In a number of cells, low concentrations of the DHP Ca^{2+} antagonists actually enhanced the transient LVA current before subsequently blocking at higher concentrations. This ability of DHP compounds to act as both an agonist and

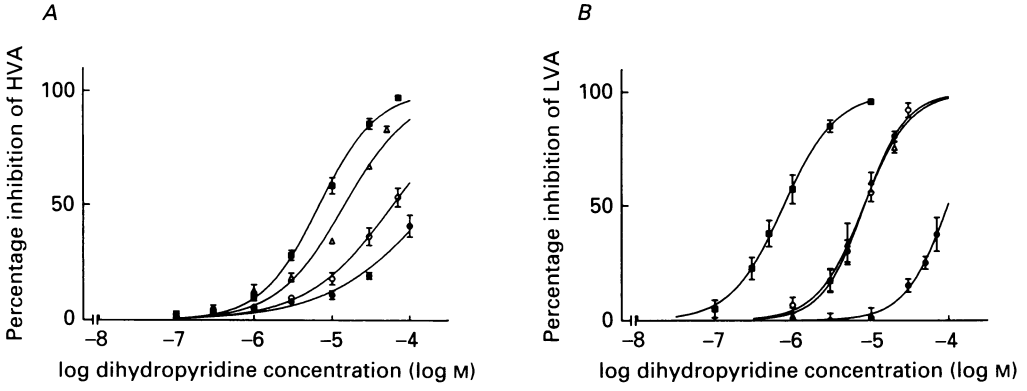

Fig. 13. Dose–response curves to dihydropyridine (DHP) calcium channel antagonists. *A*, inhibition of high-voltage-activated (HVA) current. Calcium currents were elicited every 2 min by stepping to 0 mV for 500 ms from a holding potential (V_H) of −80 mV. Dose–response curves were constructed by measuring the percentage inhibition of the sustained component of I_{Ca} in the presence of increasing concentrations of nicardipine (■), nitrendipine (△), nimodipine (○) and nifedipine (●). All measurements were made after subtraction of the leak current recorded in the presence of 200 μM Cd^{2+}. All data points are the means ± S.E.M. of between four and eight cells. Due to the limited solubility and low potency of the DHP compounds on the HVA current it was only possible to construct a full dose–response curve for nicardipine. Fitting the data for nicardipine by least-squares non-linear regression gave an IC_{50} concentration of 6·9 μM, a Hill slope of 1·1 and a correlation coefficient (r^2) of 0·998. An estimate of the IC_{50} values for the other DHPs was made by fitting the available data using non-linear regression to a hyperbolic function with the minimum and maximum values constrained to 0 and 100% respectively. This yielded theoretical IC_{50} values (determined by extrapolation) of *14·5 μM (slope = 1·0, r^2 = 0·979), *60·8 μM (slope = 0·8, r^2 = 0·997) and *203 μM (slope = 0·6, r^2 = 0·963) for nitrendipine, nimodipine and nifedipine, respectively. *B*, effects of DHPs on the transient LVA current. Currents were evoked every 30 s by stepping to −30 mV for 200 ms from V_H = −80 mV. Dose–response curves were fitted as described above and all data points are means ± S.E.M. of three to six cells. The IC_{50} values for nicardipine, nitrendipine, nimodipine and *nifedipine on the LVA current were 0·773 μM (slope = 1·3, r^2 = 0·991), 8·24 μM (slope = 1·46, r^2 = 0·993), 8·24 μM (slope = 1·61, r^2 = 0·995) and *97·5 μM (slope = 1·55, r^2 = 0·994) respectively. (* IC_{50} values determined by extrapolation.)

an antagonist has been observed in a number of other preparations and may reflect the racemic nature of the compounds (see Scott *et al.* 1991).

The voltage dependence of the current blocked by the different DHPs was examined by constructing *I–V* curves. All of the DHP Ca^{2+} antagonists inhibited the T-type LVA current (see above and Fig. 13*B*) resulting in a reduction in the amplitude of the hump (at around −30 mV) in the descending limb of the peak current *I–V* curve (not shown). Figure 12*C* shows a typical effect of nicardipine on the *I–V* plot for sustained HVA current. The block was largely voltage independent with the nicardipine-sensitive current being indistinguishable from the control

current on the basis of either its threshold or peak potential (Fig. 12*D*). Unlike nicardipine, the other DHPs displayed some voltage dependence to their block with greatest inhibition occurring at strongly depolarized potentials (more positive than −10 mV). However, this was not very pronounced and rarely resulted in more than a 2–3 mV negative shift in the peak of the *I–V* curve.

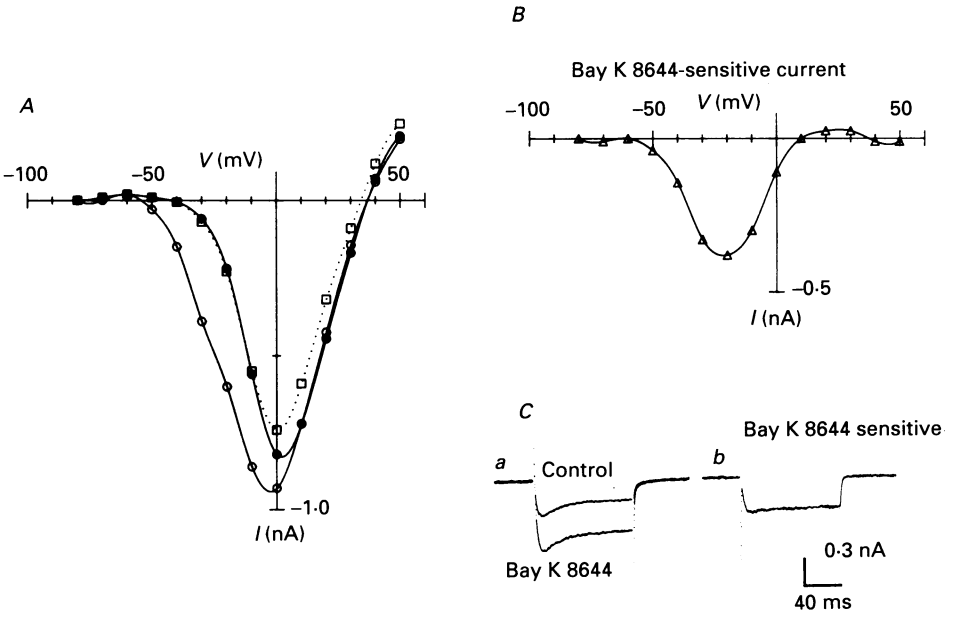

Fig. 14. The actions of the dihydropyridine agonist Bay K 8644 and antagonist nifedipine on the whole-cell calcium current (I_{Ca}) in rat basal forebrain neurones. *I–V* curves were constructed by imposing depolarizing voltage steps of 100 ms duration in 10 mV increments from a holding potential (V_H) of −80 mV once every 30 s. *A*, *I–V* plots of the sustained component of I_{Ca} measured at the end of each step, under control conditions (●), in the presence of 3 μM Bay K 8644 (○) and in the presence of 3 μM Bay K 8644 and 1 μM nifedipine (□). The enhancement of the current produced by Bay K 8644 was voltage dependent, being most pronounced at hyperpolarized potentials with little or no effect at membrane potentials > +10 mV: the effect of this was to shift the peak of the *I–V* relationship by approximately −5 mV. Subsequent addition of nifedipine (1 μM) in the continued presence of Bay K 8644 almost totally abolished the Bay K 8644-enhanced current but produced little inhibition of the current below control values. *B*, an *I–V* plot of the digitally subtracted Bay K 8644-sensitive component of the current for the same cell. The current threshold was around −60 mV and reached a peak at approximately −20 mV. *Ca*, control and Bay K 8644-enhanced currents for the cell shown in *A* and *B* evoked using a test depolarization to −20 mV (V_H = −80 mV). *Cb*, the Bay K 8644-sensitive current obtained by subtracting the two traces shown in *a*. The current exhibits little or no decay during the course of the 100 ms step.

Bay K 8644

This compound selectively enhances DHP-sensitive currents (Bean, 1989; Scott *et al.* 1991). In basal forebrain neurones, Bay K 8644 ($\leqslant 3$ μM) produced a small enhancement of the maximum calcium current, (mean increase 11·3 ± 2·5%; $n = 6$). Examination of the *I–V* relationship for the calcium current revealed that

Bay K 8644 enhanced I_{Ca} at test potentials between −65 and 0 mV, with little or no effect at more depolarized potentials, and caused a 4–5 mV shift to the left in the peak of the *I–V* curve (Fig. 14*A*). The amplitude of the Bay K 8644-sensitive current was maximal at −20 mV (Fig. 14*B*) and the enhanced current was largely sustained displaying almost no inactivation during the voltage command (Fig. 14*C*). In contrast to effects to the sustained HVA current. Bay K 8644 did not augment the transient LVA current, whilst at high concentrations ($\geqslant 10$ μM) racemic Bay K 8644 inhibited all components of I_{Ca}.

Effects of DHP Ca^{2+} antagonists in the presence of Bay K 8644

Most interestingly the HVA current enhanced by Bay K 8644 was inhibited more effectively by DHP Ca^{2+} antagonists than was the normal HVA current. Thus concentrations of nifedipine as low as 1–5 μm were capable of fully reversing the effect of Bay K 8644 (Fig. 14*A*), whereas concentrations at least 10 times higher were needed to inhibit the normal current to any appreciable extent (see Fig. 13*A* and above).

It is noteworthy that in many cells even in the absence of Bay K 8644, a small component of the sustained current (< 100 pA) activated at −30 mV could also be more readily blocked by DHP Ca^{2+} antagonists than was the principal HVA current or the transient LVA current. The amplitude of this component was too small to allow full quantitation. However, at concentrations too low to affect the principal HVA current (1 μM), the rank order of potency against this current component was nifedipine > nicardipine > nitrendipine = nimodipine. This is quite different from that against either the HVA current or the transient component of LVA current (Fig. 13).

DISCUSSION

In common with many other mammalian neurones (Bean, 1989; Scott *et al.* 1991), the magnocellular cholinergic basal forebrain neurones studied in these experiments exhibited at least two kinetically distinct Ca^{2+} currents: a transient, low threshold (LVA) current, and a more sustained (but still inactivating) higher threshold (HVA) current. However, whilst these Ca^{2+} currents in basal forebrain neurones were in many ways similar to those reported in other cells, they did show some unusual properties.

LVA current

The transient LVA current was similar to the T-type current described in several other cells, with highly voltage-dependent activation and inactivation processes (Carbone & Lux, 1984, 1987; Fox, Nowycky & Tsien, 1987*a*; Chen & Hess, 1990). However, it was strikingly different from that in other central neurones in another respect: namely, it exhibited almost no steady-state inactivation at resting membrane potential (−70 to −75 mV). This arises from a combination of an unusually positive half-inactivation potential (about −50 mV) and a very steep inactivation curve (slope factor 3·8 mV). By comparison, reported values for the LVA half-inactivation potential and slope factors in other central neurones range

between −76 and −94 mV and between 6·3 and 8·3 mV (Coulter, Huguenard & Prince, 1989; Thompson & Wong, 1991; Fraser & MacVicar, 1991; Regan, 1991). This means that the LVA current might have a more prominent influence on both normal excitability and resting Ca^{2+} influx than in other central neurones.

A second interesting aspect of the forebrain LVA current concerns its pharmacology. While it resembles T-type LVA currents in its sensitivity to divalent cations (high sensitivity to Ni^{2+} coupled with low sensitivity to Cd^{2+}) it displayed an unexpectedly high sensitivity to dihydropyridine Ca^{2+} antagonists – most notably, to nicardipine: this blocked the LVA current at submicromolar concentrations, and indeed was more effective against the LVA current than against the HVA current. This clearly differs from the properties usually associated with the T-type LVA current in peripheral neurones (Nilius, Hess, Lansman & Tsien, 1985; Fox *et al.* 1987*a*). Akaike *et al.* (1989) have reported that the LVA current in hypothalamic neurones can also be blocked by DHP compounds, but in these cells all the DHP compounds exhibited similar potencies, with K_D (dissociation constant) values within the range 3·5–7 μM. By contrast, in basal forebrain neurones there was a 100-fold difference in the relative potencies of nicardipine and nifedipine (see Fig. 13*B*). The question of the DHP sensitivity of these (and other) central neurones is discussed further below.

HVA current

The HVA current in basal forebrain neurones exhibited complex kinetics. Thus, during long (0·5 s) voltage commands, the current showed a bi-exponential inactivating component superimposed on a more sustained pedestal current. An obvious possibility is that the macroscopic HVA current is carried by two (or more) different channel types with different inactivation rates, equivalent to the N- and L-type originally described in sensory neurones (Nowycky, Fox & Tsien, 1985; Fox *et al.* 1987*b*). However, this particular subdivision does not seem to explain the complex kinetics of the HVA current in basal forebrain neurones, since ω-CgTX, which selectively inhibits the N-type current in sensory ganglion cells (Aosaki & Kasai, 1989), reduced a proportion of the HVA current (about 40%) but did not materially alter the inactivation kinetics of the residual current. Thus the complex kinetics of the macroscopic current are not necessarily indicative of kinetically different types of HVA channel. Indeed, studies of both L- and N-type channels have revealed that a single conductance channel is capable of producing both inactivating and non-inactivating currents (Plummer & Hess, 1991; Slesinger & Lansman, 1991) so the transient and pedestal currents may simply arise as the result of the channels switching between these two modes of activity.

In contrast, there is much more compelling evidence for the presence of *pharmacologically* different HVA channels. Some 40% of the macroscopic HVA current was blocked by ω-CgTX; this presumably corresponds to the component of current carried by 'N'-type channels reported in other cells (Aosaki & Kasai, 1989; Plummer, Logothetis & Hess, 1989). However, while the residual current *could* be blocked by dihydropyridines, the concentrations of DHPs required were very high (up to 100 μM nifedipine), and effective DHP concentrations blocked all components of current, including both the ω-CgTX-sensitive HVA current and the LVA current. Indeed, block by DHPs showed a monotonic increase with increasing concentration,

without any clear evidence for a specific DHP-sensitive component. For this reason, it seems unlikely that the ω-CgTX-resistant HVA current was a truly DHP-sensitive 'L'-current. It might be argued that this apparent insensitivity of the HVA current is merely a result of the voltage dependence of DHP block (Bean, 1984) since we used a negative holding potential (−80 mV). However, the additional current induced by Bay K 8644 also activated from the same holding potential was very much more sensitive to DHPs, being totally blocked by 1 μM nifedipine (Fig. 14*A*): if this represents the true 'L'-current, then clearly a current which is only blocked at 100 μM nifedipine is not the L-current.

Several other central neurones appear to possess a component of HVA current resistant to both ω-CgTX and DHPs (Regan, Sah & Bean, 1991). Likewise, Ca^{2+} channels expressed from rat brain mRNA in oocytes are insensitive to DHPs (Leonard, Nargeot, Snutch, Davidson & Lester, 1987). In Purkinje cells, a current of this type has been reported to be blocked by venom from the funnel web spider (Llinás, Sugimoro, Lin & Cherksey, 1989). We have not yet tested this: the specific fraction of this venom responsible for block is not yet widely available, and none of the constituents so far extracted have proved selective for the non-ω-CgTX- and non-DHP-sensitive component of current (Adams, Bindokas, Dolphin & Scott, 1989; Bindokas & Adams, 1989; Mintz, Venema, Adams & Bean, 1991). Instead, we find that we can quite selectively block the ω-CgTX-insensitive component of the current using low concentrations of the trivalent cations Gd^{3+} or La^{3+}. Of these, Gd^{3+} appeared to be the more potent and selective. It should be noted that the action of Gd^{3+} differed quite clearly from that of Cd^{2+} (which blocked ω-CgTX-sensitive and -insensitive components of HVA current with equal facility) or Ni^{2+} (which preferentially blocked the LVA current). Docherty (1988) has previously reported that Gd^{3+} appeared to block a kinetically distinct component of the HVA current in NG108-15 neuroblastoma hybrid cells, in the sense that the Gd^{3+}-sensitive component of the current assessed by subtraction showed a unique mono-exponential decay with a different time constant from that of the control current, and which superficially resembled the decay kinetics of the N-type current. We find essentially the same characteristics on the Gd^{3+}-sensitive component of current in basal forebrain cells, but this clearly does *not* equate with the N-current in so far as exactly the same amount of current is blocked by Gd^{3+} in the absence and presence of ω-CgTX. Thus, it is not clear whether the current component blocked by Gd^{3+} does indeed exhibit unique kinetics: the change in decay kinetics might equally be expected to result from the rate constants of the open-channel block described by Lansman (1990; k_{on} 3·2 M^{-1} s^{-1}, k_{off} 34 s^{-1} at 0 mV). In contrast the much faster rate constant for Cd^{2+} (Lansman, Hess & Tsien, 1986) implies that block by Cd^{2+} will be essentially at equilibrium throughout the command, and would thus not be expected to alter the kinetics of the current within the temporal resolution of the recording.

Notwithstanding, the end result is that there appear to be at least three pharmacologically distinguishable components to the calcium current in magnocellular basal forebrain neurones; an LVA current, selectively blocked by Ni^{2+}, and two HVA components, selectively blocked by ω-CgTX and Gd^{3+} respectively; and that a substantial proportion of the total current can be eliminated by a judicious combination of the three. This should prove useful in further analyses of the functions of these three components.

This work was supported by the Medical Research Council.

REFERENCES

ADAMS, M. E., BINDOKAS, V. P., DOLPHIN, A. C. & SCOTT, R. H. (1989). The inhibition of Ca^{2+} channel currents in cultured neonatal rat dorsal horn ganglion (DRG) neurones by ω-Agatoxin-1A (funnel-web-spider toxin). *Journal of Physiology* **418**, 34*P*.

AKAIKE, N., KOSTYUK, P. G. & OSIPCHUK, Y. V. (1989). Dihydropyridine-sensitive low-threshold calcium channels in isolated rat hypothalamic neurones. *Journal of Physiology* **412**, 181–195.

ALVAREZ DE TOLEDO, G. & LÓPEZ-BARNEO, J. (1988). Ionic basis of the differential neuronal activity of guinea-pig septal nucleus studied *in vitro*. *Journal of Physiology* **396**, 399–415.

AOSAKI, T. & KASAI, H. (1989). Characterisation of two kinds of high voltage-activated Ca-channel currents in chick sensory neurones. Differential sensitivity to dihydropyridines and ω-conotoxin GVIA. *Pflügers Archiv* **414**, 150–156.

BEAN, B. P. (1984). Nitrendipine block of cardiac calcium channels: high-affinity binding to the inactivated state. *Proceedings of the National Academy of Sciences of the USA* **81**, 6388–6392.

BEAN, B. P. (1989). Classes of calcium channels in vertebrate cells. *Annual Review of Physiology* **51**, 367–384.

BINDOKAS, V. P. & ADAMS, M. E. (1989). ω-Aga-I: presynaptic calcium channel antagonist from venom of the funnel web spider, *Agelenopsis asperta*. *Journal of Neurobiology* **20**, 171–188.

CARBONE, E. & LUX, H. D. (1984). A low-voltage-activated fully inactivating Ca channel in vertebrate sensory neurones. *Nature* **310**, 501–502.

CARBONE, E. & LUX, H. D. (1987). Kinetics and selectivity of a low-voltage-activated calcium current in chick and rat sensory neurones. *Journal of Physiology* **386**, 547–570.

CASTELLANO, A. & LÓPEZ-BARNEO, J. (1991). Sodium and calcium currents in dispersed mammalian septal neurons. *Journal of General Physiology* **97**, 303–320.

CHEN, C. & HESS, P. (1990). Mechanisms of gating of T-type calcium channels. *Journal of General Physiology* **96**, 603–630.

CHOI, D. W. (1988). Calcium-mediated neurotoxicity: relationship to specific channel types and role in ischemia damage. *Trends in Neurosciences* **11**, 465–469.

COULTER, D. A., HUGUENARD, J. R. & PRINCE, D. A. (1989). Calcium currents in rat thalamocortical relay neurones: Kinetic properties of the transient low-threshold current. *Journal of Physiology* **414**, 587–604.

COYLE, J. T., PRICE, D. L. & DELONG, M. R. (1983). Alzheimer's disease: a disorder of cortical innervation. *Science* **219**, 1184–1189.

DOCHERTY, R. J. (1988). Gadolinium selectively blocks a component of calcium current in rodent neuroblastoma × glioma (NG108–15) cells. *Journal of Physiology* **298**, 33–47.

DREYER, E. B., KAISER, P. K., OFFERMANN, J. T. & LIPTON, S. A. (1990). HIV-1 coat protein neurotoxicity prevented by calcium channel antagonists. *Science* **248**, 364–367.

FOX, A. P., NOWYCKY, M. C. & TSIEN, R. W. (1987*a*). Kinetics and pharmacological properties distinguishing three types of calcium currents in chick sensory neurones. *Journal of Physiology* **394**, 149–172.

FOX, A. P., NOWYCKY, M. C. & TSIEN, R. W. (1987*b*). Single channel recordings of three calcium channels in chick sensory neurones. *Journal of Physiology* **394**, 173–200.

FRASER, D. D. & MACVICAR, B. A. (1991). Low-threshold calcium current in rat hippocampal lacunosum-moleculare interneurons: Kinetics and modulation by neurotransmitters. *Journal of Neuroscience* **11**, 2812–2820.

GRIFFITH, W. H. (1988). Membrane properties of cell types within guinea-pig basal forebrain nuclei in vitro. *Journal of Neurophysiology* **59**, 1590–1612.

GRIFFITH, W. H. & MATTHEWS, R. T. (1986). Electrophysiology of AChE-positive neurons in basal forebrain slices. *Neuroscience Letters* **71**, 169–174.

HAMILL, O. P., MARTY, A., NEHER, E., SAKMANN, B. & SIGWORTH, F. (1981). Improved patch-clamp techniques for high-resistance recording from cells and cell-free membrane patches. *Pflügers Archiv* **391**, 85–100.

HEDREEN, J. C., BACON, S. J. & PRICE, D. L. (1985). A modified histochemical technique to visualize acetylcholinesterase-containing axons. *Journal of Histochemistry and Cytochemistry* **33**, 134–140.

KAY, A. R. & WONG, R. K. S. (1986). Isolation of neurones suitable for patch clamping from adult mammalian central nervous system. *Journal of Neuroscience Methods* **16**, 227–238.

LANSMAN, J. B. (1990). Blockade of current through single calcium channels by trivalent lanthanide cations. *Journal of General Physiology* **95**, 679–696.

LANSMAN, J. B., HESS, P. & TSIEN, R. W. (1986). Blockade of current through single calcium channels by Cd^{2+}, Mg^{2+} and Ca^{2+}. *Journal of General Physiology* **38**, 321–347.

LEONARD, J. P., NARGEOT, J., SNUTCH, T. P., DAVIDSON, N. & LESTER, H. A. (1987). Ca channels induced in *Xenopus* oocytes by rat brain mRNA. *Journal of Neuroscience* **7**, 875–881.

LLINÁS, R. R., SUGIMORI, M., LIN, J.-W. & CHERKSEY, B. (1989). Blocking and isolation of a calcium channel from neurons in mammals and cephalopods utilizing a toxin fraction (FTX) from funnel-web spider poison. *Proceedings of the National Academic Sciences of the USA* **86**, 1689–1693.

LÓPEZ-BARNEO, J., ALVAREZ DE TOLEDO, G. & YAROM, Y. (1985). Electrophysiological properties of guinea-pig septal neurones in vitro. *Brain Research* **347**, 358–362.

MCKINNEY, M., COYLE, J. T. & HEDREEN, J. C. (1983). Topographic analysis of the innervation of the rat neocortex and hippocampus by the forebrain cholinergic system. *Journal of Comparative Neurology* **217**, 103–121.

MATTHEWS, R. T. & LEE, W. L. (1991). A comparison of extracellular and intracellular recordings from medial septum/diagonal band neurons in vitro. *Neuroscience* **42**, 451–462.

MESULAM, M.-M., ELLIOTT, J. M., LEVEY, A. I. & WAINER, B. H. (1983). Cholinergic innervation of cortex by basal forebrain: cytochemistry and cortical connections of the septal area, diagonal band nuclei, nucleus basalis (substantia innominata), and hypothalamus in the rhesus monkey. *Journal of Comparative Neurology* **214**, 170–197.

MINTZ, I. M., VENEMA, V. J., ADAMS, M. E. & BEAN, B. P. (1991). Inhibition of N- and L-type Ca^{2+} channels by the spider venom toxin ω-Aga-IIIA. *Proceedings of the National Academy of Sciences of the USA* **88**, 6628–6631.

NAKAJIMA, Y., NAKAJIMA, S., OBATA, K., CARLSON, C. G. & YAMAGUCHI, K. (1985). Dissociated cell culture of cholinergic neurons from nucleus basalis of Meynert and other basal forebrain nuclei. *Proceedings of the National Academy of Sciences of the USA* **82**, 6325–6329.

NILIUS, B., HESS, P., LANSMAN, J. B. & TSIEN, R. W. (1985). A novel type of cardiac calcium channel in ventricular cells. *Nature* **316**, 443–446.

NOWYCKY, M. C., FOX, A. P. & TSIEN, R. W. (1985). Three types of neuronal calcium currents with different calcium agonist sensitivity. *Nature* **316**, 440–443.

OHMORI, H. & YOSHII, M. (1977). Surface potential reflected in both gating and permeation mechanism of sodium and calcium channels of the tunicate egg cell membrane. *Journal of Physiology* **267**, 429–463.

PLUMMER, M. R. & HESS, P. (1991). Reversible uncoupling of inactivation in N-type calcium channels. *Nature* **351**, 653–659.

PLUMMER, M. R., LOGOTHETIS, D. E. & HESS, P. (1989). Elementary properties and pharmacological sensitivities of calcium channels in mammalian peripheral neurons. *Neuron* **2**, 1453–1463.

PORTZEHL, H., CALDWELL, P. C. & RÜEGG, J. C. (1964). The dependence of contraction of muscle fibres from the crab *Maia squinado* on the internal concentration of free calcium ions. *Biochimica et Biophysica Acta* **79**, 581–591.

REGAN, L. J. (1991). Voltage-dependent calcium currents in Purkinje cells from rat cerebellar vermis. *Journal of Neuroscience* **11**, 2259–2269.

REGAN, L. J., SAH, D. W. Y. & BEAN, B. P. (1991). Ca^{2+} channels in rat central and peripheral neurons: High-threshold current resistant to dihydropyridine blockers and ω-conotoxin. *Neuron* **6**, 269–280.

RICHARD, S., DIOCHOT, S., NARGEOT, J., BALDY-MOULINIER, M. & VALMIER, J. (1991). Inhibition of T-type calcium currents by dihydropyridines in mouse embryonic dorsal root ganglion neurones. *Neuroscience Letters* **132**, 229–234.

SCOTT, R. H., PEARSON, H. A. & DOLPHIN, A. C. (1991). Aspects of vertebrate neuronal voltage-activated calcium currents and their regulation. *Progress in Neurobiology* **36**, 485–520.

SEGAL, M. (1986). Properties of rat medial septal neurones recorded *in vitro*. *Journal of Physiology* **379**, 309–330.

SHER, E. & CLEMENTI, F. (1991). Omega-conotoxin-sensitive voltage operated calcium channels in vertebrate cells. *Neuroscience* **42**, 301–307.

SIMS, N. R., BOWEN, D. M., ALLEN, S. J., SMITH, C. C. T., NEARY, D., THOMAS, D. J. & Davison, A. N. (1983). Presynaptic cholinergic dysfunction in patients with dementia. *Journal of Neurochemistry* **40**, 503–509.

SLESINGER, P. A. & LANSMAN, J. B. (1991). Inactivating and non-inactivating dihydropyridine-sensitive Ca^{2+} channels in mouse cerebellar granule cells. *Journal of Physiology* **439**, 301–323.

THOMPSON, S. M. & WONG, R. K. S. (1991). Development of calcium current subtypes in isolated hippocampal pyramidal cells. *Journal of Physiology* **439**, 671–689.